# Near-Continuous Monitoring of a Coastal Salt Marsh Margin: Implications to Predicting Marsh Edge Erosion

**Jack A. Cadigan[1*], Navid H. Jafari[2], Nan Wang[3], Qin Chen[4], Ling Zhu[5], Brian D. Harris[6] Cameron E. Markowitz[7]**

[1*]Jack A. Cadigan, Clayton Doctoral Fellow, Department of Civil and Environmental Engineering, Louisiana State University, Patrick F. Taylor Hall, Baton Rouge, LA 70803, Phone: (225) 578-8442, ORCID ID: 0000-0002-1200-8275. Email: jcadig1@gmail.com

[2]Navid H. Jafari, Ph.D., Assistant Professor, Department of Civil and Environmental Engineering, Louisiana State University, 3212D Patrick F. Taylor Hall, Baton Rouge, LA 70803, Office: (225)578-8475, Fax: (225)578-4945, Email: njafari@lsu.edu

[3]Nan Wang, Ph.D. Candidate , Department of Civil and Environmental Engineering, Northeastern University, 400 SN, Boston, MA 02115, Office: (617)373-5465, Email: wang.nan@northeastern.edu

[4]Qin Chen, Ph.D., Professor, Department of Civil Engineering, Northeastern University, 471 SN, Boston, MA 02115, Office: (617)373-5465, Email: q.chen@northeastern.edu

[5]Ling Zhu, Ph.D., Associate Research Scientist, Department of Civil Engineering, Northeastern University, 400 SN, Boston, MA 02115, Office: (617)373-5465, ORCID ID: 0000-0003-0261-6848. Email: l.zhu@northeastern.edu

[6]Brian D. Harris, Ph.D. Candidate , Department of Civil and Environmental Engineering, Louisiana State University, 3212D Patrick F. Taylor Hall, Baton Rouge, LA 70803, Office: (225)578-8475, Fax: (225)578-4945, ORCID ID: 0000-0001-5771-1880. Email: bharr96@lsu.edu

[7]Cameron E. Markowitz, Project Engineer, Stantec Consulting Services, 6900 Professional Pkwy E, Sarasota, FL 34240, Phone: (941) 907-6900, Email: cameron.markowitz@stantec.com

Corresponding author: Jack Cadigan (jcadig1@lsu.edu)

**Key Points:**

- A near-continous marsh erosion monitoring system using photographic cameras is presented.
- Daily erosion data shows most marsh-edge erosion occurs due to repeated, low-energy wave events.
- Short-term erosion rates are slightly higher than satellite derived rates, with implications to coastal restoration projects.

## Abstract

Mechanisms that control marsh edge erosion include wind-generated waves, vegetation, mudflats, anthropogenic factors, and geotechnical properties of sediments. However, existing models for predicting marsh edge evolution focus primarily on edge retreat rates as a function of wave energy while accounting for other controlling factors as empirical constants. This simplification rises from a lack of high frequency monitoring of marsh evolutions. In particular, marsh erosion is time-scale dependent and conducting field observations on short time and spatial scales could elucidate the progression of erosion, which may improve marsh erosion predictive models. This study developed and validated a near continuous camera monitoring system to document marsh edge erosion at a high frequency in Terrebonne Bay, Louisiana. Erosion pins were monitored with the cameras and daily erosion rates were estimated. This was supplemented with daily wave power to explore the relationships between daily erosion and wave power. The largest magnitude erosion events are driven by a buildup in wave energy over a seven-day time period coupled with a strong one-day wave event, indicating a gradual reduction in marsh edge resistance with continued wave attack. Long-term erosion monitoring methods, including monthly field visits, smooths over the large magnitude short-term erosion events. For example, satellite and aerial imagery provide a long period of record, but they seem to underestimate the average annual erosion rate in the region, the effect of which may become exasperated over the varying temporal scales considered in the planning efforts of projects meant to protect the Louisiana coastline.



## Plain Language Summary

A near-continous camera monitoring system was installed along a marsh edge in a rapidly eroding coastal Louisiana salt-marsh. A daily scale erosion dataset was derived from the camera system and is used to examine relationships between wave power and edge erosion. Results indicate erosion varies seasonally and large erosion events occur due to energy buildup caused by repeated wave attack rather than strong one-time events. Erosion rates from various methods are compared and show that some methodology may underestimate erosion rates, with implications to coastal restoration projects meant to protect the Louisiana coastline.


## 1 Introduction

Located at the interface between marine and terrestrial environments, salt marshes dissipate wave energy (Chen and Zhao 2011; Moller et al. 2014), provide a unique habitat for many flora and faunal species, filter nutrients and sediments from the water column, enhance carbon sequestration over decennial and millennial time scales (Zedler

and Kercher 2005), and increase fishery production in the areas which surround them (Cheong et al. 2013). Despite their societal value, the salt marsh edge or shoreline is vulnerable to erosion with respect to storm activity or wave action (e.g., Schwimmer and Pizzuto 2000; Marani et al. 2011; Mariotti and Fagherazzi 2013; Ganju et al. 2013; Bendoni et al. 2014; Leonardi and Fagherazzi 2014). The mechanisms that control marsh edge erosion include wind-generated waves (Fagherazzi et al. 2006; Mariotti and Fagherazzi 2010), vegetation (van de Koppel et al. 2005; D'Alpaos et al. 2007), cohesive mudflats (Black et al., 2002; Amos et al., 2010), anthropogenic factors (Gedan et al., 2009), and geotechnical properties of sediments (Feagin et al., 2009; Howes et al., 2010; Jafari et al. 2019). Existing models for predicting marsh edge evolution focus primarily on edge retreat rates as a function of wave energy while accounting for other controlling factors, e.g., soil and vegetation properties, into empirical constants (see Table 1). They predict annual marsh retreat by correlating observed erosion rates (aerial imagery, erosion pins, RTK and UAV surveys) with predicted wave characteristics (as a function of water level and wave power), across a range of analytical parametric wind models and computational models using SWAN (Schwimmer 2001; Marani et al. 2011; Priestas et al. 2015; Leonardi and Fagherazzi 2015; Mariotti and Fagherazzi; Johnson 2016; Bendoni et al. 2019; Everett et al. 2019).

Beyond semi-empirical predictive models, laboratory- and field-derived mechanistic models investigate particular failure modes observed in wave flume experiments or from field monitoring (Bendoni et al. 2014; Gabet 1998; Bendoni et al. 2016). For example, Bendoni et al. (2014) instrumented vegetated and unvegetated cohesive sediments in a wave flume to replicate the toppling mass failure due to oscillating waves, and found the dynamic response and pore-water pressure generation of the soil system also appears to be an important factor in predicting bank instability. The field-derived model by Gabet (1998) replicates the undercutting failure mechanism for estuaries in San Francisco, California using the momentum equilibrium between the weight of the block and soil-vegetation shear strength. Bendoni et al. (2016) developed a model from field observations to predict erosion of root mat and underlying sediment layers individually based on the still water level and wave characteristics while incorporating soil erodibility properties and wave power into the undercutting failure mechanism. If the lower sediment layer retreats at a faster rate than the vegetated layer, undercutting will form and eventually leads to a mass failure when a threshold length is exceeded. This model also accounts for the still water level, where the top face only erodes when the still water level is at or above the height of the toe face.

Given the advancements in mechanistic and empirical marsh-edge retreat rate models, accurate predictions of marsh edge erosion remain elusive. For coastal Louisiana, Allison et al. (2017) compiled historical retreat rates using remote sensing, wave power derived from wind records, and marsh properties (type, bulk density, and vegetation) across 1,343 points and found a weak correlation. The high scatter was attributed to several reasons, including a lack of knowledge of the mobilized failure mode and corresponding mechanistic formulations, missing input parameters (e.g., geotechnical, ecological, marsh profile), and temporal incompatibility. The mechanistic models discussed herein (Bendoni et al. 2014, Gabet 1998, Bendoni et al. 2016) capture two failure modes (undercutting and surficial soil erodibility) at varying degrees of complexity. These models highlight the need to account for the failure mode, as undercutting failure is found to control the retreat rate. Leonardi and Fagherazzi (2015), Johnson (2016), and Sanford and Gao (2017) represent the first models to incorporate shear strength in their formulations. The marsh profile can also play an influential role, e.g., the marsh platform and mudflat elevations control the wave power estimates. Thus, there is a need for models that include geotechnics (shear strength, soil damping from waves), ecology (vegetation type, roots), and marsh profile in the semi-empirical models. Bendoni et al. (2016) compared short-term (weeks to months) to long-term (years to decades) retreat rates reported by Marani et al. (2011) and found the short-term rates to be much higher. They explained this observation using the analogy to the dependence of the rate of bed load transport on sampling frequency described by Singh et al. (2009). Longer time scale observations tend to smooth out higher peak fluctuations and include both variations intrinsic to the physical processes at work and possible changes in external forcing (e.g., due to human activities or climate change). Moreover, Wang et al. (2017) investigated salt marsh erosion from large-scale (estuary) to mesocosm scale (sediment erosion, vegetation, wave interaction) and found that wave exposure influences on a larger spatial scale, while soil and vegetation properties are more impactful on the local scale. This temporal incompatibility suggests that marsh erosion is also time scale dependent and conducting field observations on short time and spatial scales could elucidate the progression of erosion and failure mechanism.

A step towards developing process-based, mechanistic models for investigating short- and long-term marsh edge erosion is to increase the field observational frequency such that the progression of failure can be documented. The majority of wetland monitoring is focused on the elevation evolution (Temmerman et al. 2003; Kirwan and Murray 2007), while only few studies continuously observe the landward transgression. As a result, the specific mechanisms and causes of marsh retreat (e.g., mass failures and particle-by-particle erosion) due to wind

118 waves are not well understood (Gabet 1998; Schwimmer 2001; Gedan et al. 2009; Marani et al. 2011). While there
119 are an increasing number of studies using physical experiments for simulating marsh environments (e.g., Coops et
120 al. 1996; Chen et al. 2013; Feagin et al. 2009; Francalanci et al. 2015; Bendoni et al. 2015), a potential drawback of
121 the small-scale physical models is the temporal incompatibility, i.e., the experiment duration is much shorter than
122 processes in the field. Field reconnaissance of coastal marsh erosion is predominantly focused on measuring
123 boundary retreat rates from aerial imagery, total station and prism rod, GPS units, and erosion pins. The site visits
124 are also spaced 1 to 4 months apart, so extensive monitoring to identify the progression of marsh failure is not
125 feasible. Time-lapse still and motion imagery include a wealth of visible details for the observation of soil behavior,
126 infrequent and extreme events in ecology, geology, and meteorology (Newbery and Southwell 2009; Holman et al.
127 2003). For example, Zhang et al. (2014) installed low power and low cost networked smart cameras to document the
128 short-term processes of bluff erosion. Accordingly, the objective of this study was to develop and validate a near-
129 continuous camera monitoring system in Terrebonne Bay, Louisiana to document marsh edge erosion, and
130 subsequently analyze the archived images to visualize and quantify the evolution of marsh edge erosion. The
131 scientific questions regarding the progression of marsh edge erosion are discussed herein: (1) What is the failure
132 mechanism; (2) How rapidly is erosion occurring; (3) Is the erosion tied to infrequent extreme forcings or more
133 frequent lower-energy events; and (4) Is it linked to any predictable physical or meteorological event?

134 ## 2 Physical Setting

135 The study site is located in Terrebonne Bay, Louisiana, approximately 97 km southwest of the city of New Orleans
136 (Fig. 1) and is accessible by a ~15 minute boat transit from the Louisiana University Marine Consortium
137 (LUMCON). Terrebonne Bay is sediment starved, receiving no fluvial inflow (Everett et al. 2019; Twilley et al.
138 2016; Bentley et al. 2015), and is separated from the Gulf of Mexico by two barrier island chains (Inoue and
139 Wiseman 2000; Watzke 2004). The site is predominantly characterized by highly compressible and soft silts and
140 clays in the shallow strata deposited during the Lafourche period of the Mississippi River Delta, approximately
141 2500-300 years B.P. (USACE 1958; Penland et al. 1988). Following significant river engineering activity in the
142 1950s, 24.5% of Terrebonne basin converted to open water (Rodriguez et al. 2020), and has accounted for
143 approximately 25% of the total wetland lost in coastal Louisiana between 1932-2010 (Couvillion et al. 2011). In
144 1981, the life expectancy of Terrebonne Bay wetlands was estimated to be 102 years (approximately the year 2083)
145 with a conservative land loss rate of 27.8 $km^2$/yr calcuated using data from 1890-1978 acting on the remaining 2832

146 $km^2$ of land (Gagliano et al. 1981; Wells 1996). Restreppo (2019) suggests with more recent observations that the
147 marsh platform may be under sea-level by approximately 2035. However, this prediction uses a simplistic model
148 relying on site-specific marsh platform elevation, sediment accumulation rates, and relative sea-level rates, assuming
149 changes in the aforementioned parameters remain constant with time and ignoring marsh edge erosion. The region
150 is characterized by relatively low-wave energy wave events though wave energy may increase by orders of
151 magnitude due to the passages of strong storm events, including cold fronts and hurricanes (Coleman 1988; Culling
152 2018). Water levels in Terrebonne Bay average 1.7 m in depth, with a maximum depth of 3 m (Everett et al. 2019).
153 The study site features a microtidal and diurnal tide, which ranges in amplitude from 0.1 to 0.6 m, depending on
154 equatorial or tropical tides (Everett et al. 2019; Leonard and Luther 1995). March is typically the most energetic
155 month for waves in Terrebonne Bay (Everett et al. 2019), and thus is expected to produce the highest erosion rates.

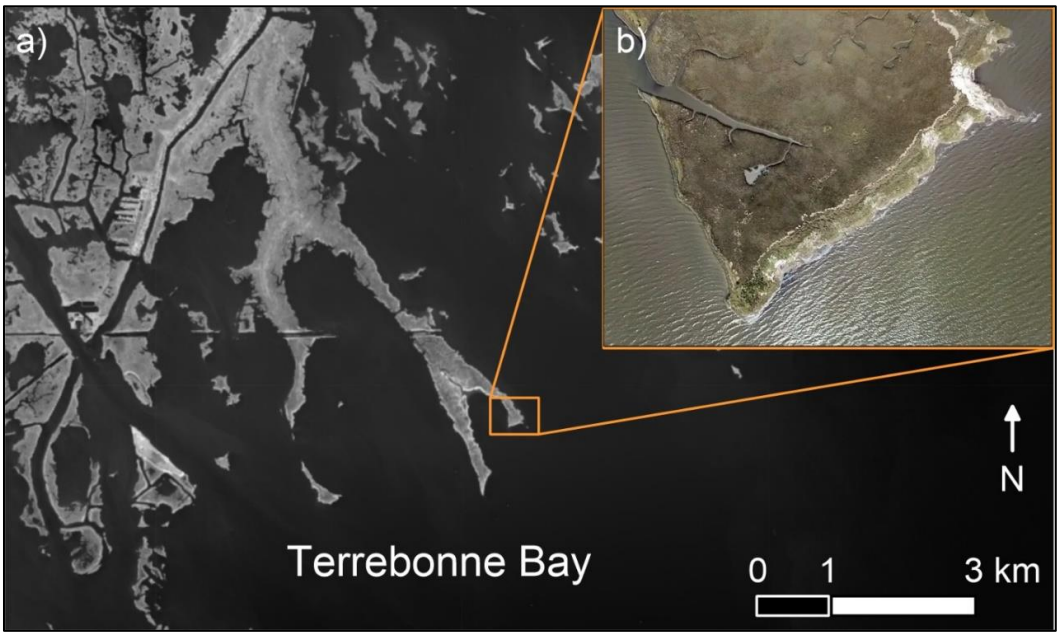


156
157 **Figure 1.** (a) Overview of the study site in Terrebonne Boy located in coastal Louisiana (Base
158 image: USDA Forestry Service), and (b) drone imagery of study site.

159 ## 3 Materials and Methods

160 ### 3.1 Marsh Erosion Pins

161 Time-lapse imagery was captured at five (5) minute intervals over continuous twelve (12) hour periods daily from
162 March 2018 to February 2020. Several lapses in coverage occurred due to camera malfunctions (e.g., saltwater
163 corrosion) intermittently as a result of strong storm events. Multiple times after severe storms, the interior
164 components of the cameras were discovered to be coated in muddy sediments. To that end, several iterations of

camera layout were implemented to avoid damage from wave attack while balancing adequate data collection. The image data acquisition system is composed of a Moultrie all-weather outdoor game-camera mounted on a stainless steel channel and ten (10) sets of 182 cm (6 ft) length erosion pins spaced laterally in even increments of one meter across the marsh edge. Each pin was inserted to a known reference length, with 18 cm of visible reflective marking exposed as an initial benchmark for photogrammetric analysis. At each pin location, two erosion pins were inserted into the marsh edge (Fig. 2d). In particular, the top pin was inserted into the vegetated mat and is referred to as the "vegetation pin", while the bottom pin was inserted into the lower unvegetated soil and is referred to as the "soil pin".

The camera images were downloaded approximately monthly dependent on site access. During a site visit, the erosion pins were manually measured using a meter stick to the nearest 1 cm, and the difference in exposed length was recorded as the total erosion for the period. Following a site visit, the raw data images that tracked the exposed lengths of each pin were transferred from the camera SD card to a laboratory computer for analysis. Erosion was determined by measuring the number of pixels in the initial image corresponding to the benchmark exposed pin length of 18 cm and comparing the number of pixels in each subsequent image. To avoid issues with pin orientation relative to the location and angle of the camera, each pin was individually measured with a separate initial benchmark length. Erosion was then quantified as the difference between the exposed length at the beginning and end of the analysis period. The number of images collected during each period varied due to the dependence on site conditions, i.e. tide, storm passages, visibility.

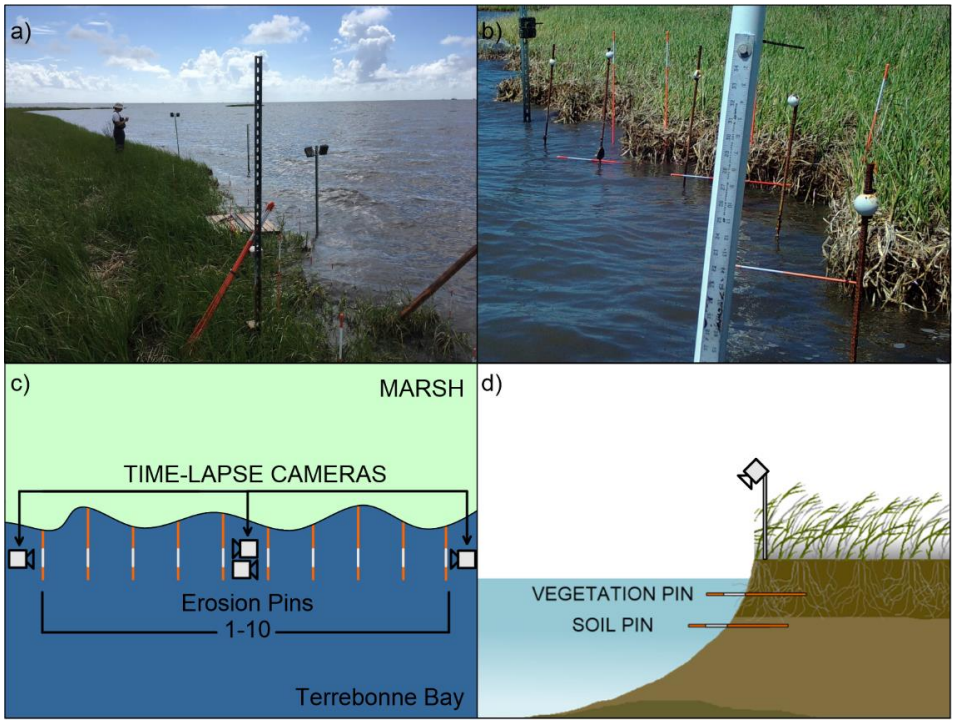


**Figure 2.** (a) Installing the continuous erosion measurement system, (b) example image showing protruding erosion pins, (c) schematic plan view of the camera and erosion pin layout, and (d) schematic cross-section of erosion pin monitoring system with vegetation and soil pins.

### 3.2 Wave Power Modelling

SWAN is a third-generation spectral wave model used to predict wind wave generation and transformation in coastal waters (Booij et al. 2004). The model solves the wave action balance equation (Eq. 1) to calculate the wave spectral evolution in temporal, geographical, and spectral spaces (Booij et al. 1999):

$$\frac{\partial N}{\partial t} + \frac{\partial (C_{gx} N)}{\partial x} + \frac{\partial (C_{gy} N)}{\partial y} + \frac{\partial (C_{g\sigma} N)}{\partial \sigma} + \frac{\delta (C_{g\theta} N)}{\delta \theta} = \frac{S}{\sigma} \#(1)$$

where $N$ is the wave action density, $t$ is the time, $(x, y)$ are horizontal Cartesian coordinates, $\theta$ is the wave direction taken counterclockwise from the geographical east, $\sigma$ is intrinsic radian frequency. $C_{gx}$, $C_{gy}$, $C_{g\sigma}$, and $C_{g\theta}$ denote the speeds of energy propagation in the $x$-space, $y$-space, $\sigma$-space, and $\theta$-space, respectively. On the right-hand side, S represents the source terms representing the effects of generation, dissipation, and non-linear wave-wave interactions (Chen et al. 2005).

In this study, the SWAN model simulated wave conditions driven by local wind and ocean swell in Terrebonne Bay. The model physics implemented include white capping, depth-limited wave breaking, bottom friction, refraction, diffraction, quadruplet interactions, and triad interactions. The model domain and the model

setup are the same as Everett et al. (2019). The water level boundary condition is obtained from Grand Isle, LA station of National Oceanic and Atmospheric Administration (NOAA). For the wind forcing, the LUML1 station located at LUMCON inside Terrebonne Bay is used in the SWAN model. The wind and water level forcings are applied uniformly over the entire model domain. To incorporate the swell energy into the SWAN model, an offshore wave boundary condition was applied along the seaward boundary of the model domain, which was obtained from United States Army Corps of Engineers (USACE) Wave Information Studies (WIS) station 73125, and from the output of a Gulf of Mexico wave model (Abolfazli et al. 2020). The wind data from January to April and from July to November 2019 is missing at LUML1 due to damage caused by cold fronts and Hurricane Barry (July 2019), so an artificial neural network trained with the wind measurements at the NOAA stations at Grand Isle and Amerada Pass, and at LUML1 was used to fill the gaps of the missing wind data.

The time series of the significant wave height $H_s$ and peak wave period $T_p$ output from the SWAN model was used to calculate wave bulk wave power $P$.

$$P = \frac{\rho g H_s^2}{16} C_g \#(2)$$

where $C_g$ is the wave group velocity and $\rho$ is the water density. The bulk wave power is the raw wave power calculated at each time step, regardless of whether the water level exceeds the marsh surface elevation or falls below the toe of the marsh edge.

The effective wave power is the underlying hydrodynamic forcing that drives marsh edge erosion (McLoughlin et al. 2015; Tonelli et al. 2010), and was recently calculated to provide a majority of the wave attack on the marsh edge in Terrebonne Bay (Everett et al. 2019). The effective wave power also accounts for periods that the marsh edge is considered to be safe from wave attack when the water level is either below the scarp bottom or when the water levels exceed a threshold elevation above the marsh platform. Effective wave power is filtered using a range of water levels to account for these lower and upper thresholds, with the upper and lower limits of the effective range defined as $H_s$ above Mean High Water (0.3244m NAVD88) and $H_s$ below Mean Low Water (0.0850 m NAVD88), respectively. Otherwise, the effective wave power is set as zero at that time step (Everett et al. 2019).

### 3.3 Regression Analyses

Quantification of the relationship between wave power and marsh-edge erosion was performed using statistical analyses conducted in MATLAB® 2020a (Mathworks 2020). Datasets were imported as time-tables at varying

temporal resolutions (e.g., minutes-days), with wave power as daily averaged values, and camera erosion at varying intervals on the minute scale (e.g. 5-60 minutes). The data was merged into one table using the built-in 'synchronize' function. Linear regression analysis was performed using bisquare weighting to minimize the effect of outliers on the regression while fitting the majority of the data (Fox and Weisberg 2011). The integrated weekly wave power is computed using the trapezoid rule with a running 7-day window, including the day that the measured erosion is being compared. The 7-day window was chosen based on allowing short term cold front storms and longer term hurricane storm events to completely cycle through the site. Integrated weekly wave powers should be considered reflective of the degraded resistance of the marsh edge to several smaller-scale wave power events over a one-week period.

### 3.4 Aerial Imagery

To compare long term erosion rates measured using satellite and aerial imagery (Ozesmi and Bauer 2002; Prigent et al. 2001), USGS Landsat 8 and USDA National Agricultural Imagery Program aerial imagery were accessed using the Google Earth Engine (Gorelick et al. 2017; USDA 2020; USGS 2020). Geo-located imagery was downloaded and imported to GIS software where average erosion rates between periods were calculated. The average erosion rates were computed for a period bounded between 1989 and 2019. Due to the need to account for varying pixel-resolution of satellite imagery, atmospheric conditions, and sea-state at the time of image acquisition, the erosion rates are considered as approximate estimates for comparison to more accurate measured field rates using the camera system.

## 4 Results

Fig. 3 shows the relationship between the measured erosion using the photogrammetric system and the erosion manually measured using the meterstick. The number of comparisons points available are limited by the temporal resolution of field measured erosion rates, along with the issue that the erosion pins were underwater in several field visits and cameras could fail before the field visit. The dashed line in Figure 3 represents a perfect fit between the camera measured erosion and the field measured erosion. The data point pairs lie closely to the unity-slope line, with

an average difference of approximately 3 cm. As a result, Fig. 3 substantiates that the camera system provides erosion measurements similar to those measured in the field but with significantly higher temporal resolution.

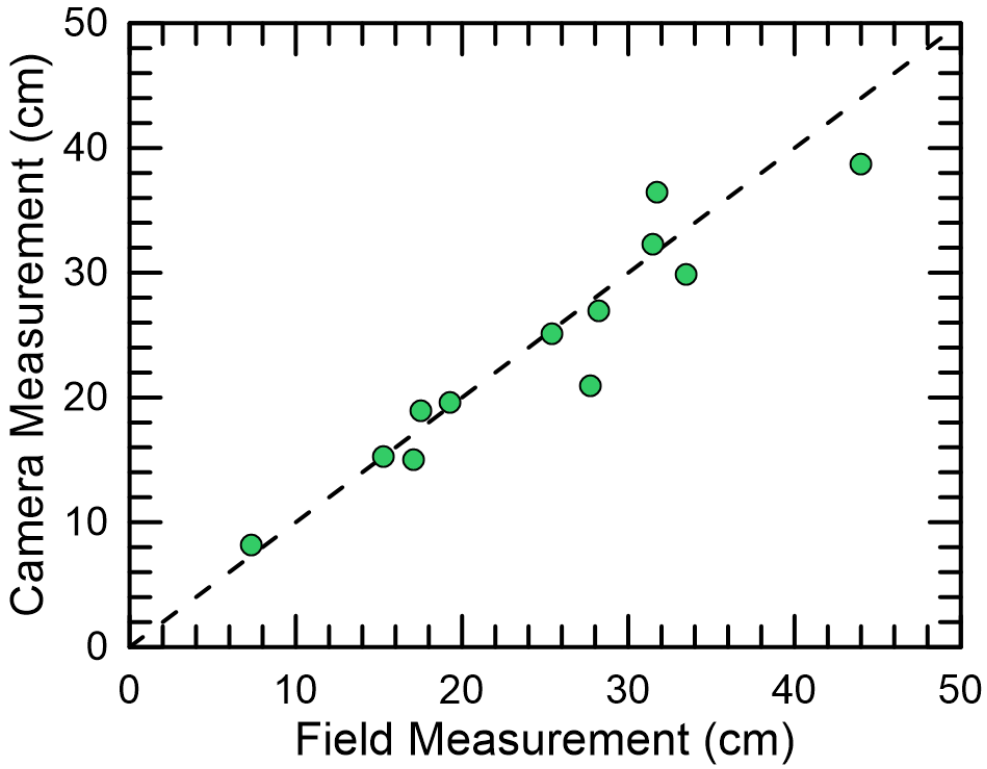


**Figure 3.** Comparison of manual field measurement and the camera system erosion.

Fig. 4 shows the relationship between the field measured erosion for the pins inserted into the vegetated mat and the underlying unvegetated organic soils. The vegetated pins in Fig. 4a generally lie between 20-80 cm of erosion between each time period. While several vegetation pins are outliers (specifically pin #1), the majority exhibit similar trends and are bounded between 300-600 cm of cumulative erosion (Fig. 4c). The soil pins in Fig. 4b and 4d show a similar pattern, but the magnitude of erosion is slightly lower. For example, an average of 350 cm cumulative erosion was observed for the soil pins compared to the average of 450 cm cumulative erosion for the vegetated pins. The benefit of the camera system was direct observation of the progression of erosion, which showed that erosion events followed waves directly impacting the vegetation root mat rather than the underlying soil, due to the elevated water levels at the site. The pin locations experience fluctuating levels of erosion over the span of the study period, without one specific location consistently experiencing higher or lower levels of erosion than any other. The trend of cumulative erosion suggests that erosion occurs in episodic events because the rise in slope occurs during specific time periods. For example, a large spike in cumulative erosion is observed first in the period of April 2018 to July 2018, and again from April 2019 to July 2019. This period corresponds to the spring months

where cold front passages are frequent, especially since the month of March is typically the most energetic month for waves in Terrebonne Bay (Everett et al. 2019).

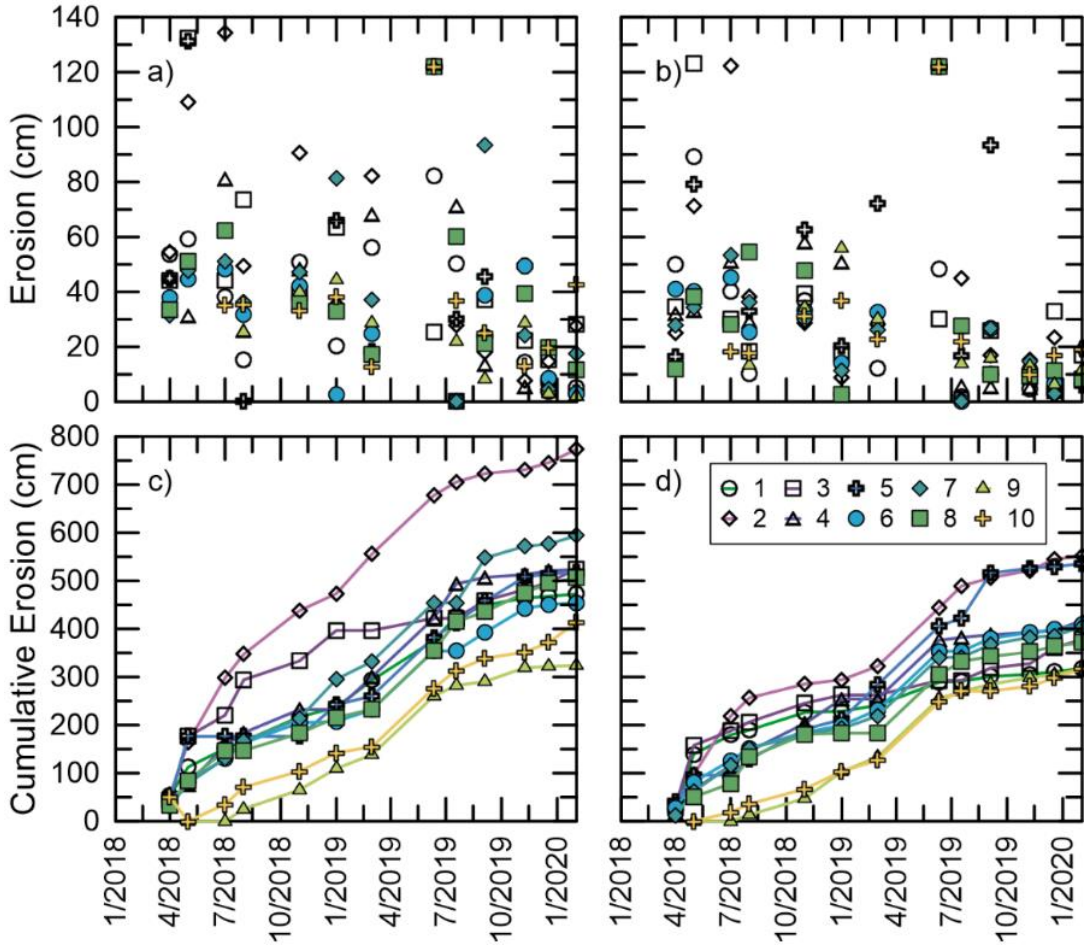


**Figure 4.** Recorded erosion from the ten (a) vegetation pins, (b) soil pins, and the cumulative erosion for (c) vegetation pins and (d) soil pins.

The average annual erosion rate for the manually obtained soil and vegetation pins are shown in Fig. 5. The annual erosion rates were extrapolated to an annual value by dividing the total erosion over the number of days in the time period, and then multiplied by 365.25 days to obtain an annualized erosion rate. The vegetated mat layer shows higher erosion rates across the span of the whole study, but the rates are similar for most periods measured. The overall average rate for the site fluctuates between 1-3 m/year. The maximum annual erosion rate occurs in the Spring 2018 with values up to 9 m/yr. A similar peak was observed in the Spring 2019, but the annual retreat rate is lower because it averages the erosion from March to beginning of July. Two major gaps in the data are present around January-February 2019 due to damage from a strong cold front passage, as well as a gap after Hurricane

Barry in July 2019. The range of values encapsulates shoreline retreat areas recently calculated for a different reach of wetlands in Terrebonne Bay by Mealncon et al. (2013), though is significantly higher in magnitude than those reported by Watzke (2004). Annual erosion rates decrease during the summer months and is at a minimum during the winter. As a result, Fig. 5 clearly demonstrates that the erosion rate varies seasonally and depending on the time periods forecasted an annual or average rate may not accurately capture the true erosional patterns. While there is great uncertainty involved with projecting storm trends into the future, as evidenced by the varying predictions in literature, the general consensus is that there will likely be an increase of seasonal extreme storm events in the future due to the effects of climate change (Vecchi et al. 2008; Bender et al. 2010; Knutson et al. 2010; Mousavi et al. 2010; Emmanuel 2013; Grinsted et al. 2013; CPRA 2017b), not only should retreat rates increase but the seasonal effect may become more pronounced. As more marsh is also eroded, the swell or fetch concomitantly increases and hence could lead to a positive feedback loop that further accelerates marsh edge erosion.

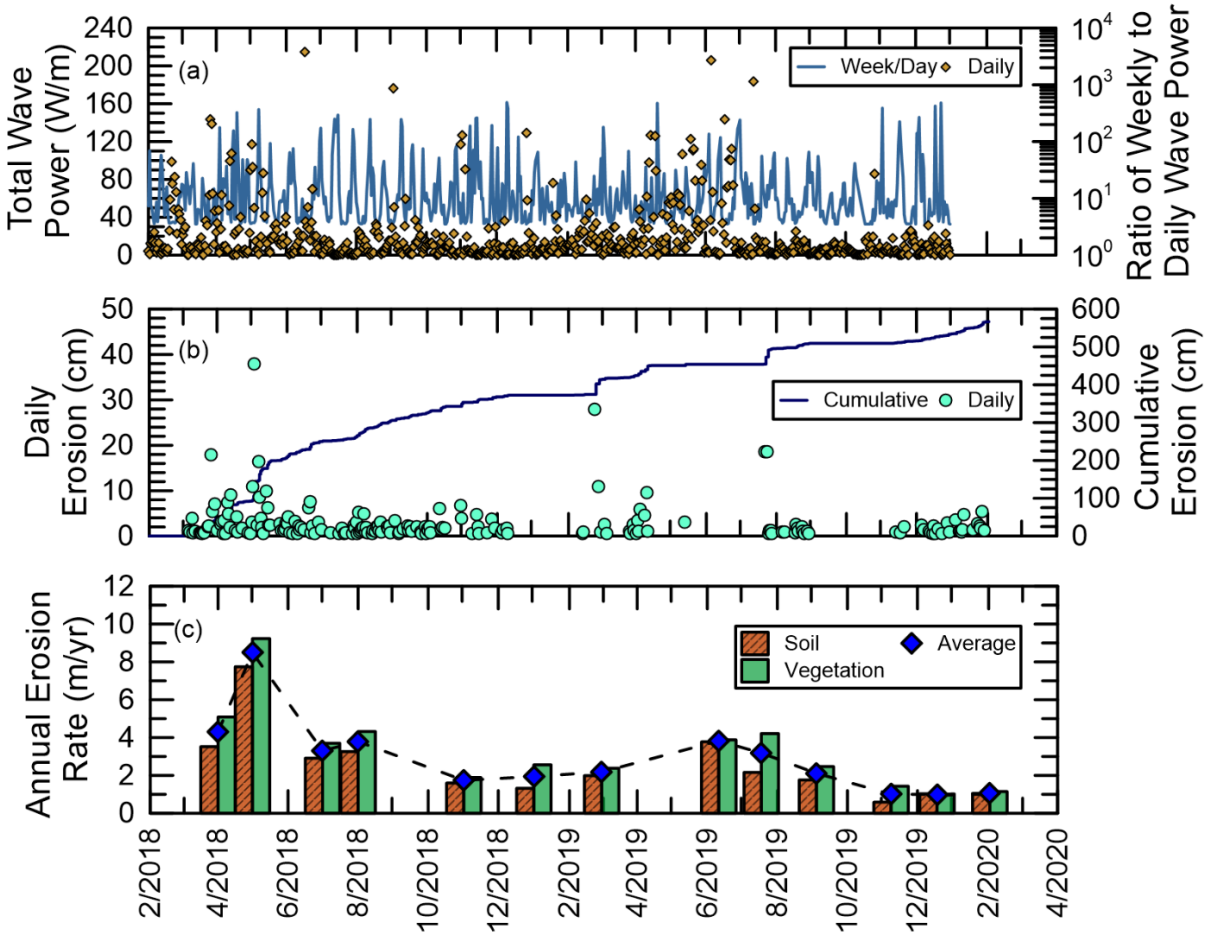


**Figure 5.** (a) Total wave power and the ratio of weekly to daily wave power, (b) daily and cumulative erosion values, (c) annual erosion rates extrapolated from field measurements.

The wave power results are displayed in Fig. 5(a). The daily wave power is predominantly below 75 W/m, with occasional spikes nearing 150 W/m. The ratio of weekly to daily wave power shows the running build-up effect of daily wave events, resulting in weekly wave power values \ up to 900x the daily wave power value. Fig. 5(b) shows the erosion measured using the camera system. The daily erosion in Fig. 5(b) features several large-erosion events between 20 to 40 cm in a single day, which correspond to time periods which experienced multiple moderate-power events in the preceding week. These erosional events caused by repeated low- to moderate-power events correspond to relatively higher weekly wave power. The majority of data points indicate that daily erosion is below 5 cm/day, further substantiating that erosion is an episodic event. The trend of the cumulative erosion curve in Fig. 5(b) depicts the effects of the large-erosion events as well as the flat nature of the curve, highlighting the more frequent and predominantly lower-erosion events.

Fig. 6 shows a comparison of the estimated annual erosion rates calculated using the camera-measured values and the field-measured values. The near-continuous nature of the camera system provides insight into the highly variable erosion rates that the marsh edge undergoes, which the less frequent monthly field visits do not capture. While the monthly measurements allow insight into the overall long-term trends, the camera measurements show the fluctuations that are present on daily scales. The large magnitude, short-term erosion events are smoothed over large time periods similar to the theory proposed by Bendoni et al. (2016). As a result, the temporal incompatibility observed in Fig. 5 along with the significant variance between daily and long-term measured erosion rates in Fig. 6 substantiates that marsh erosion is a time scale dependent process and higher frequency field observations can better capture the underlying signals causing marsh erosion.

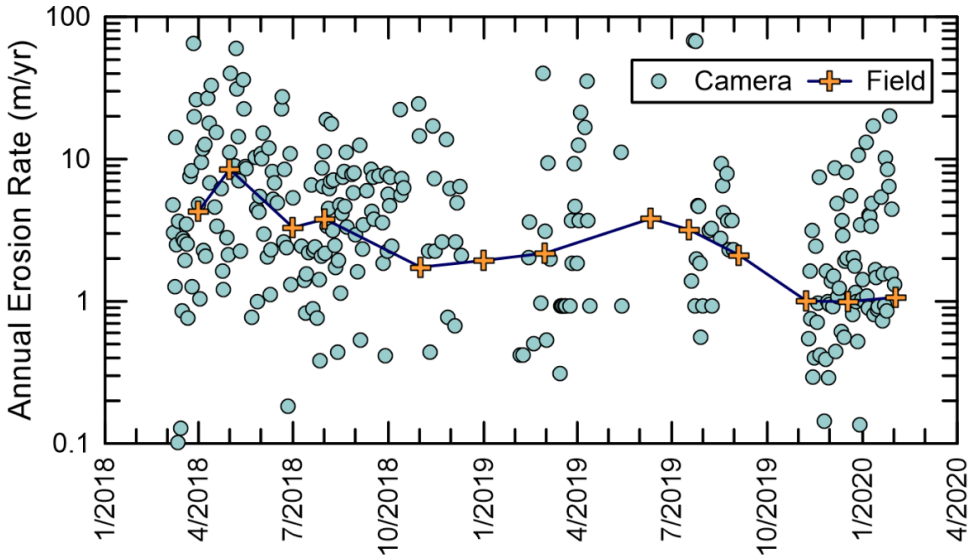


316

317 **Figure 6.** Erosion rates calculated from the camera system and field measurements.

318

319 Fig. 7 shows the regression curves for daily erosion as a function of daily and weekly wave power.
320 Logarithmic scaling is employed on all axes due to the wide spread of values for both erosion and wave power. The
321 daily and weekly wave power (Fig. 5a) both possess weak linear relations to daily erosion values, which was also
322 observed by Allison et al. (2017). The weekly wave power regression has a lower correlation coefficient (~0.11)
323 compared to the daily wave power regression (~0.18). While some of the largest daily erosion events correspond to
324 the higher ranges of wave power values, there are also large daily erosion events not directly correlated to significant
325 one-day wave power events (Fig. 7a), reinforcing the hypothesis from Leonardi et al. (2015) that strong hurricane
326 event storms are not solely responsible for all of the significant erosion in salt marshes.

327

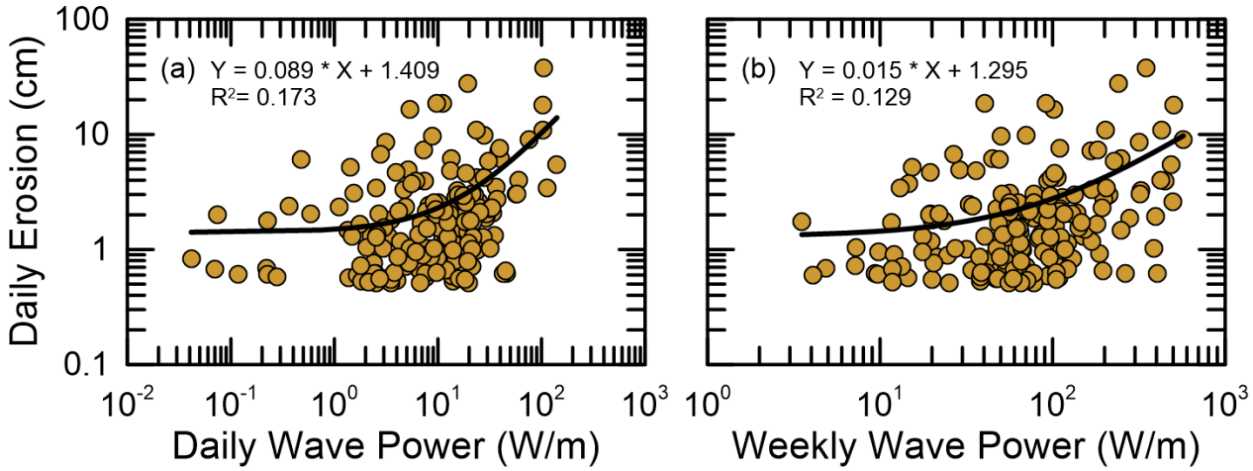


328

329 **Figure 7.** Relationships for daily erosion with (a) daily wave power, and (b) weekly wave power.

Though adequately capturing the erosion behavior of several sites internationally, the linear wave power and erosion framework proposed by Leonardi et al. (2016) does not account for the relationships present in the data in Fig. 7. The effect of time-period averaging on the Leonardi et al. (2016) linear relationship (Eq. 5) between dimensionless erosion E* (Eq. 3) and dimensionless wave power P* (Eq. 4) was investigated in Fig. 8 using daily, weekly, monthly, and three-month averages from random sets of the data. The weekly, monthly, and three-month averages are calculated using the daily measurements from the camera system and are analogous to visiting the field site to make erosion measurements at each of the respective time periods. E* is the dimensionless erosion calculated by dividing the erosion rate over the average erosion rate. P* is the dimensionless wave power, again taken by dividing wave power by the average wave power.

$$E^* = \frac{E}{E_{avg}} \#(3)$$

$$P^* = \frac{P}{P_{avg}} \#(4)$$

$$E^* = 0.67P^* \#(5)$$

The linear relationship (Eq. 5) as proposed by Leonardi et al. (2016) is superimposed over the camera erosion data transformed into E* and P* components as a comparison. The daily values in Fig. 8(a) are characterized by significant scatter, which reduces with higher values of dimensionless wave power. Weekly values in Fig. 8(b) feature significantly less scatter, with generally a closer relationship to the linear trend line from Leonardi et al. (2016). Fig. 8(c) displays the monthly averages, and Fig. 8(d) the three-month averages. With each coarsening in temporal resolution, scatter is reduced but less data is present because of larger time steps. The difference between Fig. 8 as compared to Leonardi et al. (2016), which was compiled from various wetlands around the United States, is hypothesized to be an artifact of the smoothing effect caused by measuring a total erosion value over the longer time periods between field measurements as compared to daily values.

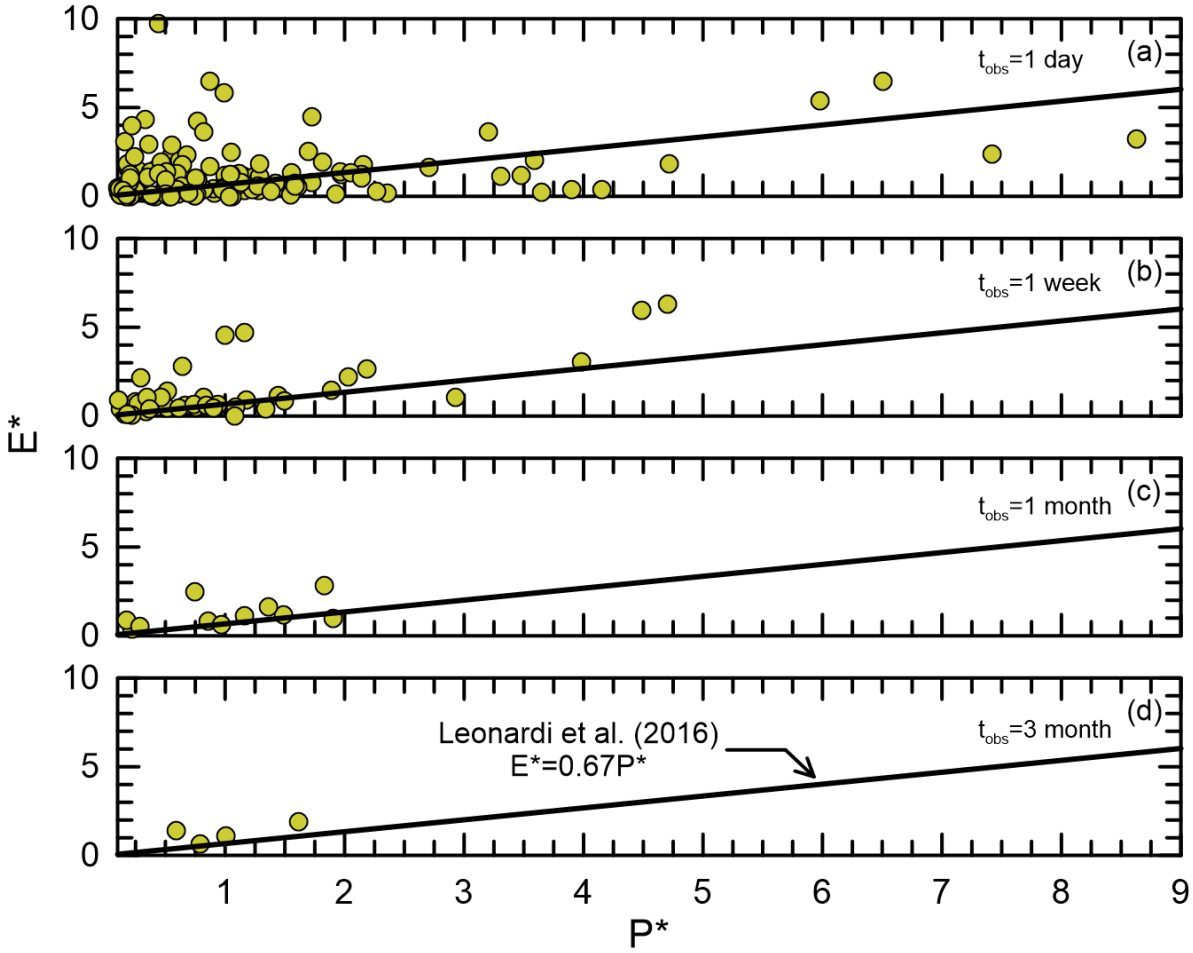


**Figure 8.** Comparison of Leonardi et al. (2016) linear fit to observed data at (a) daily time steps, (b) weekly time steps, (c) monthly time steps, (d) three-month time steps.

The lessons learned from Figs. 5-8 indicate that there is some component of short term erosion events that are not accurately captured by daily wave power values, and indicate that erosion is scale dependent temporally and spatially (Wang et al. 2017, Fagherazzi et al. 2020, Wiberg et al. 2020). Weekly wave power buildup seems to be an important signal for predicting marsh edge erosion. As a result, a heatmap of erosion as a function of short term forcing through daily wave power, as well as longer term effects through weekly integrated wave power was developed in Fig. 9. Each point represents a discrete one-day point with a triplet measurement consisting of average daily erosion, daily wave power, well as an accumulated 7-day wave power computed for the seven (7) days preceding and inclusive of the current day. Fig. 9 is divided into four quadrants, which represent distinct erosion behavior regions. Assumed threshold wave powers were selected to separate the four quadrants.

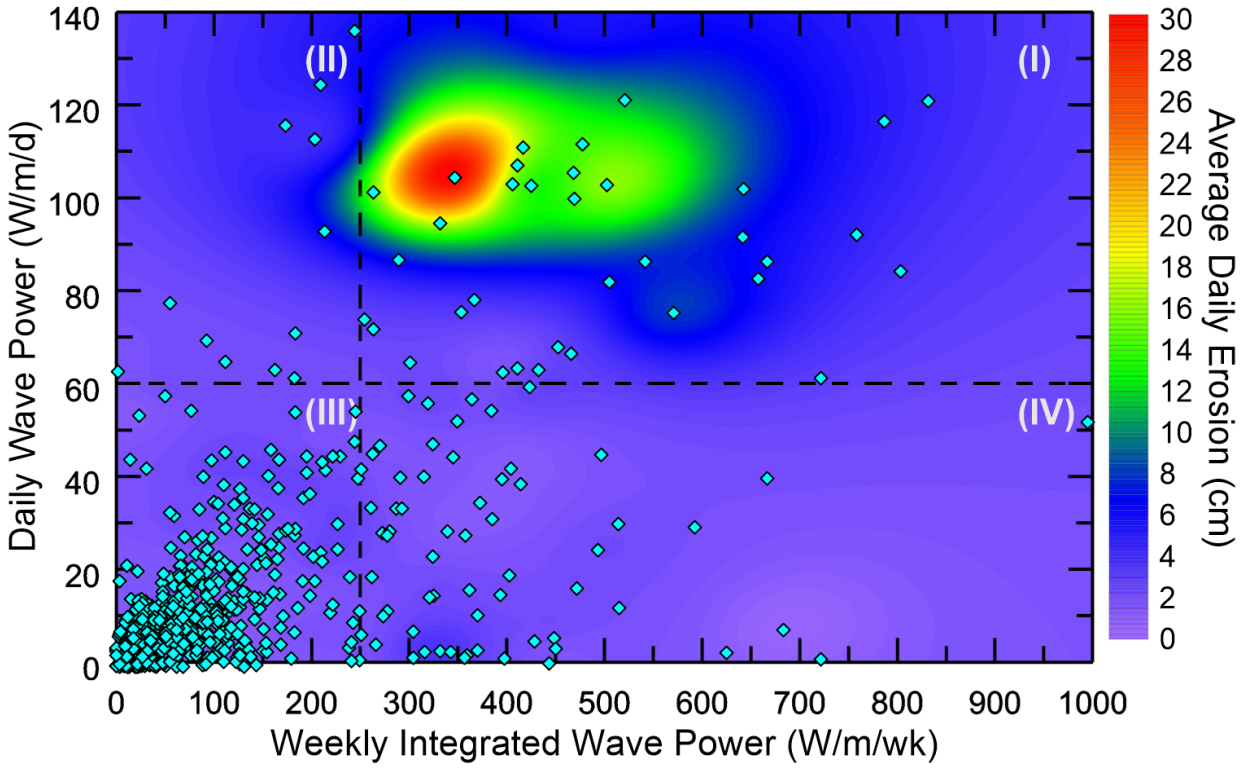


**Figure 9.** Erosion as a function of daily and weekly wave power accumulation.

Quadrant I includes the largest magnitude erosion rates, typically residing between 8 to 10 cm, with several average daily erosion values greater than 30 cm. Quadrant I is characterized by large one-day wave power events and large build-ups of accumulated weekly wave power. Fig. 10 suggests that the large erosion events are a combination of a long-term buildup of weekly wave power with a strong one-day event that triggers the erosive event. Quadrant II features points characterized by strong one-day events and relatively weak long-term buildup, indicating that the weekly buildup is likely skewed by the powerful one-day event. Most of the measured erosion and wave power triplets lie in Quadrant III, indicating low daily wave power (~0-60 W/m) and low integrated weekly wave power (~0-250 W/m). Quadrant IV features larger magnitude long-term energy buildup, but it does not include the strong one-day wave power events, which are postulated to lead to intensified erosion rates. Erosion rates in Quadrants II, III, and IV are predominantly in the range of 0 to 6 cm/day. For the salt marsh in Terrebonne Bay, the wave power thresholds that lead to intensified erosion rates are approximately a 60 W/m one-day event coupled with a 7-day buildup of at least 250 W/m.

## 5 Discussion

The objectives of this study were to explore the following four scientific questions: (1) What is the failure mechanism; (2) How rapidly is erosion occurring; (3) Is the erosion chronic or episodic; and (4) Is it linked to any predictable physical or meteorological event? The failure mechanism was observed through countless images from the camera system and the erosion pins. At this particular marsh edge, the evidence suggests that the erosion of vegetation root mat is occurring before the underlying sediment. The anecdotal evidence from multiple fields found that water levels below the marsh surface but above the root mat made forceful impacts such that the hynamic loading was felt standing on the marsh edge. Moreover, waves breaking on the edge would wash into the marsh and return at high velocity on the surface and through the pores of the vegetation roots. The breaking impact and drag from returning water could explain why the vegetation layer was eroding quicker. Alternatively, as undercutting was occasionally observed in the field, the underlying soil layer may have eroded leaving a scarp on the marsh edge. As the vegetated layer collapsed and eroded, it may have eroded to a greater magnitude than the underlying unvegetated layer. The erosion pins documented the rate of marsh retreat and further discussion is provided below on retreat rates from various techniques. The erosion pins also clearly showed that the erosion is episodic, where average daily erosion rates could approach over 10 cm/day. The observations did not find a specific event that led to erosion, although it was found that the cumulative effect of daily wave power over a period of time with at least a cold front led to higher rates of erosion.

Fig. 10 shows the average annual erosion rates estimated using aerial and satellite imagery at the study site. The dramatic erosion over relatively short time periods is clearly visible. Anecdotally the small peninsula extending from the southwest corner was connected as of early 2017. However beginning in winter 2017, the middle of the peninsula eroded until a small island formed in the bay. A comparison of erosion rates from the camera system, field visits, aerial imagery from airplanes, and satellite imagery are summarized in **Error! Reference source not found.**. The computed average erosion rates increase from approximately 2.15 m/yr for the satellite imagery to 3.15 m/yr for the camera system. The camera system captures the larger magnitude, short-term erosion events which are smoothed over when averaged (Fig. 7) over the longer-term time periods present in field visits and aerial imagery. Taking the median erosion rate of the camera data to remove the influence of significant outliers, the erosion rate falls to 2.65 m/year. While the short-term and long-term erosion rates do not match, it seems that at least in a

practical sense the long-term erosion rates are adequate even if they do not capture the true physical processes occurring.

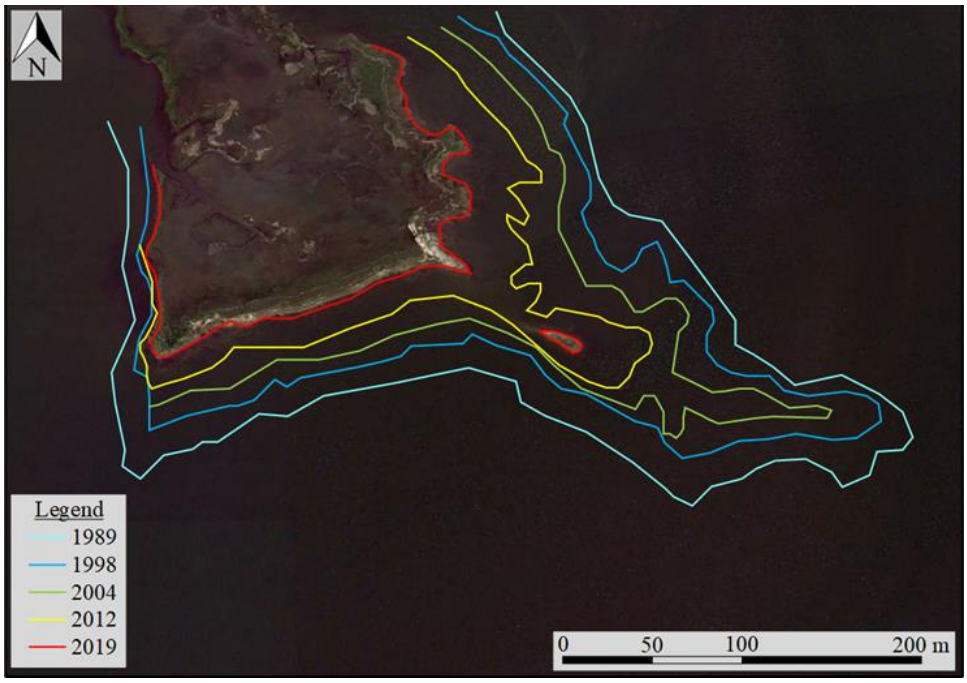


**Figure 10**. Erosion of the Terrebonne Bay marsh site from 1989-2019 derived from aerial and satellite imagery (Base image: ArcGIS, Landsat imagery courtesy of the U.S. Geological Survey, aerial imagery courtesy of the U.S.D.A. National Aerial Imagery Program).

**Table 1.** Summary of spatio-temporal coverage and resolution of techniques to monitor marsh edge erosion.

| Method | Spatial Coverage | Spatial Resolution | Measurement Type | Temporal Resolution | Erosion Rate (m/yr) |
|---|---|---|---|---|---|
| Camera System | ~1 m | ~1 cm | Near-Continuous | <1 day | 2.65 |
| Field Visit | ~10 m | ~1 cm | Discrete | 1 day | 2.80 |
| Aerial Imagery[1] | ~100 m | ~1 m | Discrete | Varies | 2.64 |
| Satellite Imagery[2] | ~1 km | ≤ 30m | Semi-Continuous | >2 weeks | 2.15 |

*(1)USDA National Aerial Imagery Program*
*(2) USGS LandSAT, Sentinel, Planet Labs*

Due to the varying scales of geomorphological processes outlined in the 2017 Louisiana Coastal Masterplan (CPRA 2017), accounting for the time-scale dependent behavior of erosion is important. For example, using the camera system derived erosion rate (2.65 m/yr) and using satellite derived erosion rates (2.15 m/yr) to estimate the value of various coastal protection projects as shown in the Masterplan would result in an estimated under-prediction of 25 m of lateral erosion over the 50-year period when relying on government satellite data. In addition, while commercial satellite imagery can obtain high resolution data ($< 1$ $m^2$) (Planet Team 2017), the resolution of government satellite imagery is still relatively course (30m x 30m) to predict erosion on a sub-basin scale (Table 1). The spatial resolution of government satellite imagery is coarser than the estimated difference in erosion predicted by the two methods in the example above. Assuming a constant retreat rate also neglects the self-reinforcing feedback by increasing fetch and depth in a shallow coastal water body. This scenario is rapidly increasing rates of marsh edge erosion in Terrebonne Bay, Barataria Bay, and Breton Sound. Moreover, applying a constant retreat rate does not account for future changes in physical conditions or the ecological responses to those conditions. Given predictions of sea-level rise and increased storm intensity, it is unlikely that physical conditions will remain constant over time and thus equally unlikely that edge erosion will occur at a constant rate in the future. This process can be visualized in Fig. 9, where increases in daily and weekly wave power will shift daily erosion points from Quadrant III towards Quadrant I and hence lead to further erosion. The implication to long-term resilience of wetlands is that more eroded material is released, which can affect marsh sediment dynamics and shoreface profile (Wilson and Allison 2008). Fig. 5(c) also shows the seasonality of marsh edge erosion, which is corroborated by observations reported in Watzke (2004), and hence shows that cold fronts play an important role in the geomorphological change of the Louisiana coast.

Currently the only effective wetland restoration technique which can keep pace with RSLR rates in coastal Louisiana are large-scale sediment diversion projects (Wang et al. 2014). Sediment diversion studies are highly dependent on temporal-scales. Thus, it is critical to understand the short-to-long term processes which will affect the erosion of newly deposited sediments (Xu et al. 2019). The importance of accurately estimating erosion rates at a variety of timescales becomes critical due to the financial investment involved in the design and implementation of restoration efforts (Pahl et al. 2020. For example, marsh edge erosion can be reduced by the installation of on-shore or off-shore protection systems. In the 2017 Coastal Master Plan, these projects were designated as shoreline protection, bank stabilization, and oyster reefs (CPRA 2017). They were implemented by adjusting the marsh edge

448 erosion rate for any part of the compartment within the influence area behind the structure. Eq. (6) was used to
449 determine the revised marsh edge erosion rate for each shoreline protection project (CPRA 2017):
450

$$MEE_{new} = \left( \left( MEE_{original} \right) \left( \frac{A_{project}}{A_{total}} \right) \left( F_r \right) \right) + \left( 1 - \left( MEE_{original} \right) \left( \frac{A_{project}}{A_{total}} \right) \right) \quad (6)$$

451
452 where $MEE_{new}$ is the marsh edge erosion rate as reduced by the project, $A_{project}$, is the project edge area, $A_{total}$ is the
453 total marsh edge area, and $F_r$ is the project reduction factor (wave attenuation rate/100%). The application of Eq. (6)
454 is underscored by the need for more accurate prediction of marsh edge retreat given the reduced wave energy by
455 shoreline protection (i.e., $F_r$), such as building rock dikes or oyster reefs. For instance, if an oyster reef project
456 reduces the annual wave power by 80%, what is the reduction of the daily and seasonal marsh edge retreat? The
457 near-continuous camera system developed and validated in this study is one technological solution.

458 ## 6 Conclusions

459 The time-lapse camera monitoring system described and presented in this study provides insight into the short- and
460 long-term processes which drive erosion events in a salt marsh in Terrebonne Bay, LA. The camera dataset of
461 erosion pins in the vegetated matt and the underlying soil layer show that the failure mechanism generally involves
462 slightly higher rates of erosion in the vegetated layer rather than the underlying sediment layer, though the erosion
463 rates are roughly the same in both layers. The largest magnitude erosion events are driven by a buildup in wave
464 energy over a seven-day time period coupled with a strong one-day wave event, indicating a gradual reduction in
465 marsh edge resistance with continued wave attack. Rather than being driven by individual strong wave events,
466 erosion occurs near continuously by relatively weaker daily wave events. The joint occurrence of both strong daily
467 wave events and large weekly buildup is rare, and is responsible for the large magnitude erosion events in the data
468 record. The long-term erosion monitoring methods, including approximately monthly field visits, smooths over the
469 large magnitude short-term erosion events. In particular, while the satellite and aerial imagery provide a long period
470 of record, they seem to underestimate the average annual erosion rate in the region, the effect of which may become
471 exasperated over the varying temporal scales considered in the planning efforts of projects meant to protect the
472 Louisiana coastline. The match presented between the camera system erosion values and field measured values
473 validates the presented methodology for a near-continuous erosion measurement system for coastal wetlands.

Further study is necessary to understand the non-linear, short-term hydro-mechanical processes behind marsh-edge erosion, along with the lack of geotechnical substrate characteristics and shear strength (Jafari et al. 2019). With the advent of sophisticated machine learning algorithms, future work could also explore artificial intelligence as a novel means to formulate marsh erosion models because it can incorporate variable datasets and at the least provide an understanding which parameters contribute more to marsh erosion and thus guide future process-based models. While machine learning is experiencing burgeoning use in geosciences to accomplish tasks such as predicting geological stratigraphy, vegetation mapping, and particularly in the oil and gas exploration field to analyze resources, it has yet to be explored towards predicting marsh erosion. As coastal wetland loss in Louisiana is the likely the result of complex interactions between many climatic, anthropogenic, and geological factors, machine learning is an ideal tool to connect all of the various erosion contributors quickly and effectively. Applying machine learning allows for a program to learn how and why these various factors interact over wide spatial and temporal scales.

## Acknowledgments, Samples, and Data

Funding for this work was provided by USACE (Cooperative Agreement W912HZ-16-2-0025). Support was provided by the Louisiana Coastal Protection and Restoration Authority (CPRA) and administered by Louisiana Sea Grant (LSG) through its Coastal Science Assistantship Program (CSAP). Support was also provided by the Department of Defense (SMART Program) and the Donald W. Clayton Ph.D.Fellowship. Suporting data for this manuscript is hosted publicly on Mendeley Data and is accessible at: http://dx.doi.org/10.17632/9fcgyw7myy.2

## References

Abolfazli, E., Liang, J., Fan, Y., Chen, Q., Walker, N., Liu, J., 2020. Surface gravity waves and their role in ocean-atmosphere coupling in the Gulf of Mexico. Journal of Geophysical Research - Oceans, revision submitted.

Arenstam, J. (2019). "The latest: Terrebonne and Lafourche wake up to Barry." The Daily Comet, Thibodaux, LA.

Bender, M. A., Knutson, T. R., Tuleya, R. E., Sirutis, J. J., Vecchi, G. A., Garner, S. T., and Held, I. M. (2010). Modeled impact of anthropogenic warming on the frequency of intense Atlantic hurricanes. Science, 327, 454-458

Bendoni, M., Mel, R., Solari, L., Lanzoni, S., Francalanci, S., and Oumeraci, H. ( 2016), Insights into lateral marsh retreat mechanism through localized field measurements, Water Resour. Res., 52, 1446– 1464, doi:10.1002/2015WR017966.

Booij, N. R. R. C., Roeland C. Ris, and Leo H. Holthuijsen. "A third-generation wave model for coastal regions: 1. Model description and validation." Journal of geophysical research: Oceans 104.C4 (1999): 7649-7666.

Chen, Q., Zhao, H., Hu, K, and Douglass, S. L, 2005. Prediction of wind waves in a shallow estuary. Journal of Waterway, Port, Coastal and Ocean Engineering, 131 (4): 137-148.

Cheong, S.-M., Silliman, B., Wong, P. P., van Wesenbeeck, B., Kim, C.-K., and Guannel, G. (2013). "Coastal adaptation with ecological engineering." Nature Climate Change, 3(9), 787-791.

Coleman, J.M. (1988). Dynamic changes and processes in the Mississippi River delta: Geological Society of America Bulletin, v. 100, no.7, p. 999-1015.

Coastal Protection and Restoration Authority. (2017b). 2017 Coastal Master Plan: C2-4: Tropical Storm Intensity and Frequency. Version Final. (p. 24). Baton Rouge, Louisiana: Coastal Protection and Restoration Authority.

Culling, D. (2018). "Shallow geologic framework, geomorphic evolution, and sand resources of a paleo-barrier shoreline, Terrebonne Bay, Louisiana, USA." Masters, Tulane University, New Orleans, LA.

Darboux, F. and Huang, C., 2003. An instantaneous-profile laser scanner to measure soil surface microtopography. Soil Science Society of America Journal, 67(1): 92–99.

Elliot, W. J., Laflen, J. M., Thomas, A. W. and Kohl, K. D., 1997. Photogrammetric and rillmeter techniques for hydraulic measurement in soil erosion studies. Transactions of the American Society of Agricultural Engineers, 40(1): 157–165.

Emanuel, K. A. (2013). Downscaling CMIP5 climate models shows increased tropical cyclone activity over the 21st century. Proceedings of the National Academy of Sciences of the U.S., 110 (30), 12219-12224.

Everett, Thomas, et al. "Quantification of Swell Energy and Its Impact on Wetlands in a Deltaic Estuary." Estuaries and Coasts 42.1 (2019): 68-84.

Fagherazzi, S., Mariotti, G., Leonardi, N., Canestrelli, A., Nardin, W., & Kearney, W. S. (2020). Salt marsh dynamics in a period of accelerated sea level rise. Journal of Geophysical Research: Earth Surface, 125, e2019JF005200. https://doi.org/10.1029/2019JF005200

Fox, J, and Weisberg, S.(2011) “Robust Regression in R An Appendix to An R Companion to Applied Regression, Second Edition.”

Gagliano, S.M., Meyer-Arendt, KJ., and Wicker, K.M., 1981. Land loss in the Mississippi River deltaic plain. Gulf Coast Assoc. Geol. Soc., Trans., 31, 295-300.

Gorelick, N., Hancher, M., Dixon, M., Ilyushchenko, S., Thau, D., & Moore, R. (2017). Google Earth Engine: Planetary-scale geospatial analysis for everyone. Remote Sensing of Environment.

Grinsted, A., Moore, J. C., and Jevrejeva, S. (2013). Projected Atlantic hurricane surge threat from rising tempe ratures, PNAS, doi:10.1073/pnas.1209980110

Gumbel, E. J. The Return Period of Flood Flows. Ann. Math. Statist. 12 (1941), no. 2, 163--190. doi:10.1214/aoms/1177731747.

Holthuijsen, L. H., et al. "SWAN Cycle III version 40.11 user manual." Delft University of Technology Press, Delft, The Netherlands (2004).

Inoue, M., and Wiseman, W. J. (2000). "Transport, Mixing and Stirring Processes in a Louisiana Estuary: A Model Study." Estuarine, Coastal and Shelf Science, 50(4), 449-466.

Jafari, N. H., Harris, B. D., Cadigan, J. A., and Chen, Q. (2019). "Piezocone penetrometer measurements in coastal Louisiana wetlands." Ecological Engineering, 127, 338-347.

Knutson, T. R., McBride, J. L., Chan, J., Emanuel, K., Holland, G., Landsea, C. ,and Held, I. (2010). Tropical cyclones and climate change. Nature Geoscience, 3, 157-163.

Leonardi, N., Ganju, N. K., & Fagherazzi, S. (2016). A linear relationship between wave power and erosion determines salt-marsh resilience to violent storms and hurricanes. Proceedings of the National Academy of Sciences of the United States of America, 113(1), 64–68. https://doi.org/10.1073/pnas.1510095112

MATLAB. (2020). version 9.8.0 (R2020a). Natick, Massachusetts: The MathWorks Inc.

McCool, D. K., Dossett, M. G., Yecha, S. J., (1981). A portable rill meter for field measurement of soil loss. Erosion and Sediment Transport Measurement (Proceedings of the Florence Symposium, June 1981). IAHS Publ. no. 133. Pullman, Washington 99164, USA. https://iahs.info/uploads/dms/iahs_133_0479.pdf

Melancon, E. J. Jr., G. P. Curole, A. M. Ledet, and Q. C. Fontenot. 2013. 2013 Operations, Maintenance, and Monitoring Report for Terrebonne Bay Shore Protection Demonstration (TE-45), Coastal Protection and Restoration Authority of Louisiana, Thibodaux, Louisiana. 75 pp. and Appendices

Mousavi, M., Irish, J. L., Frey, A. E., Olivera, F., and Edge, B. L. (2011). Global warming and hurricanes: the potential impact of hurricane intensification and sea level rise on coastal flooding. Climatic Change, 104(3/4), 575-597. doi:10.1007/s10584-009-9790-0

Myers, D.T.; Rediske, R.R.; McNair, J.N. Measuring Streambank Erosion: A Comparison of Erosion Pins, Total Station, and Terrestrial Laser Scanner. Water 2019, 11, 1846.

Ozesmi, S. L., & Bauer, M. E. (2002). Satellite remote sensing of wetlands. Wetlands ecology and management, 10(5), 381-402.

Pahl, J.W., Freeman, A.M., Raynie, R.C., Day, J., (2020). Response of the Coastal Systems to Freshwater Input with Emphasis on Mississippi River Deltaic Plain River Diversions: Synthesis of the State of the Science. Estuarine, Coastal and Shelf Science, https://doi.org/10.1016/j.ecss.2020.106866.

Pearson, C. E. (2001). "Remote-Sensing Cultural Resources Survey of the Houma Navigation Canal, Dredge Island Creation Project, Terrebonne Parish, Louisiana." USACE, ed., New Orleans District, New Orleans, LA, 68.

Penland, Shea, and John R. Suter (1983) Transgressive Coastal Facies Preserved in Barrier Island Arc Retreat Paths in the Mississippi River Delta Plain. Transactions-Gulf Coast Association of Geological Societies 33:367-381.

Penland, S., Suter, J.R., and McBride, R.A. (1987). Delta plain development and sea level history in the Terrebonne coastal region, Louisiana: Coastal Sediments (pp. 1689-1705). ASCE.

Penland, P. S. (1990). Barrier Island Evolution, Delta Plain Development, and Chenier Plain Formation in Louisiana PhD Dissert. Louisiana State University, Baton Rouge, La (1990), p. 209

Planet Team (2017). Planet Application Program Interface: In Space for Life on Earth. San Francisco, CA. https://api.planet.com.

Prigent, C., Matthews, E., Aires, F., & Rossow, W. B. (2001). Remote sensing of global wetland dynamics with multiple satellite data sets. Geophysical Research Letters, 28(24), 4631-4634.

Reed, D.J. Patterns of sediment deposition in subsiding coastal salt marshes, Terrebonne Bay, Louisiana: The role of winter storms. Estuaries 12, 222–227 (1989). https://doi.org/10.2307/1351901

Restreppo, G. A. (2019). Deltaic Wetland Dynamics from Seasonal to Centennial Scales. (Doctor of Philosophy), Louisiana State University, Baton Rouge, LA. (LSU Doctoral Dissertations 4828)

Roberts, H.H. (1985). A study of sedimentation and subsidence in the south-central coastal plain of Louisiana. United States Army Corps of Engineers, New Orleans District, New Orelans, LA. 57 pp.

Rodriguez, A. B., McKee, B. A., Miller, C. B., Bost, M. C., & Atencio, A. N. (2020). Coastal sedimentation across North America doubled in the 20th century despite river dams. Nature Communications, 11(1), 3249. https://doi.org/10.1038/s41467-020-16994-z

United States Army Corps of Engineers (1958). "Geology of the Mississippi River Deltaic Plain, Southeastern Louisiana." U.S. Army Engineer Waterways Experiment Station.

Vecchi, G. A., and T. R. Knutson, 2008: On Estimates of Historical North Atlantic Tropical Cyclone Activity. J. Climate, 21, 3580–3600, https://doi.org/10.1175/2008JCLI2178.1.

Wang, H., Steyer, G. D., Couvillion, B. R., Rybczyk, J. M., Beck, H. J., Sleavin, W. J., Meselhe, E. A., Allison, M. A., Boustany, R. G., Fischenich, C. J., and Rivera-Monroy, V. H. (2014). "Forecasting landscape effects of Mississippi River diversions on elevation and accretion in Louisiana deltaic wetlands under future environmental uncertainty scenarios." Estuarine, Coastal and Shelf Science, 138, 57-68.

Wang, H., van der Wal, D., Li, X., van Belzen, J., Herman, P. M. J., Hu, Z., Ge, Z., Zhang, L., and Bouma, T. J. (2017), Zooming in and out: Scale dependence of extrinsic and intrinsic factors affecting salt marsh erosion, J. Geophys. Res. Earth Surf., 122, 1455– 1470, doi:10.1002/2016JF004193.

Wasson, K., Ganju, N. K., Defne, Z., Endris, C., Elsey-Quirk, T., Thorne, K. M., Freeman, C. M., Guntenspergen, G., Nowacki, D. J., and Raposa, K. B. (2019). "Understanding tidal marsh trajectories: evaluation of multiple indicators of marsh persistence." Environmental Research Letters, 14(12), 124073.

Watzke, D.A. (2004). Short-term evolution of a marsh island system and the importance of cold front forcing, Terrebonne Bay, Louisiana. (Unpublished master's thesis). Department of Oceanography and Coastal Sciences, Louisiana State University, Baton Rouge, LA.

Wells, J. T. (1996). "Subsidence, Sea-Level Rise, and Wetland Loss in the Lower Mississippi River Delta." Sea-Level Rise and Coastal Subsidence: Causes, Consequences, and Strategies, J. D. Milliman, and B. U. Haq, eds., Springer Netherlands, Dordrecht, 281-311.

Wiberg, P. L., Fagherazzi, S., and Kirwan, M. L. (2020). "Improving Predictions of Salt Marsh Evolution Through Better Integration of Data and Models." Annual Review of Marine Science, 12(1), 389-413.

Xu, K., Bentley, S. J., Day, J. W., and Freeman, A. M. (2019). "A review of sediment diversion in the Mississippi River Deltaic Plain." Estuarine, Coastal and Shelf Science, 225, 106241.